PHYSICAL REVIEW B **85**, 115135 (2012)

Real-space Green's function calculations of Compton profiles

Brian A. Mattern, Gerald T. Seidler,[*] Joshua J. Kas, Joseph I. Pacold, and John J. Rehr
Department of Physics, University of Washington, Seattle, Washington 98195-1560, USA

(Received 2 February 2012; revised manuscript received 16 March 2012; published 29 March 2012)

We report the development of a first-principles, real-space Green's function method for calculation of Compton profiles in the impulse approximation. For crystalline Be, we find excellent agreement with prior theoretical treatments requiring periodicity, with prior experimental measurements of the Compton profile, and with present measurements of the dynamical structure factor via nonresonant inelastic x-ray scattering (often also called x-ray Thomson scattering in the plasma physics community). We also find good agreement with prior experimental results for the Compton profile of Cu. This approach can be extended to disordered and very high-temperature systems, such as "warm dense matter," where theories presently used for the interpretation of inelastic x-ray scattering include condensed phase effects only at a perturbative level.

DOI: 10.1103/PhysRevB.85.115135 PACS number(s): 78.70.−g

I. INTRODUCTION

Nonresonant inelastic x-ray scattering[1] (NIXS), often also called x-ray Thomson scattering (XRTS) in the plasma physics community, has long been used as a probe of material properties. For example, the Compton-scattering cross section, which is the large energy- and momentum-transfer limit of NIXS, was used in the earliest demonstrations of the particulate character of photons[2] and of Fermi-Dirac statistics.[3] Recently NIXS has seen a steady renaissance thanks to the development of third generation x-ray light sources and associated specialized x-ray spectrometers.[4–7] Recent applications address many forefront issues in condensed-matter physics,[8,9] subtle questions of bonding in chemical physics,[10–13] solvation in mixtures,[14] and long-standing problems in quantum scattering theory.[15] Because NIXS makes possible studies of low-Z edges without high-vacuum techniques, it provides an attractive alternative to, and extension of, traditional x-ray absorption spectroscopies.[16–39] More recently, NIXS experiments have yet another venue. High-power laser facilities have created a different application of NIXS, wherein laser-pumped x-ray backlighter sources allow snapshot determinations of the state variables (density and temperature) of so-called "warm dense matter" (WDM).[40–49] Our goal in this paper is to develop a quantitative treatment of the valence contribution to NIXS that is applicable in these various cases.

The wide parameter space of kinematic variables and initial states requires several different theoretical treatments of NIXS. The treatment of semicore and core levels has been solved at essentially the same level of detail as x-ray absorption fine structure and with similar tools,[23,29,30,35] whereas the theoretical treatment of NIXS involving valence excitations is still evolving. The difficulties in the latter case come from a significant sensitivity to the atomic and molecular potentials.[11,12,50–52] Hence they depend on an underlying conceptual issue: whether the scattering for given experimental conditions may be treated as nearly single-particle-like, or collective, or requiring a more sophisticated treatment of many-body effects including thermodynamic considerations.[43,45,53–57] Such issues are central to NIXS studies of the state variables of WDM.[43] The WDM sample has solidlike or sometimes higher densities but exists at temperatures that can be well in excess of the Fermi energy, and sometimes in excess of semicore and eventually core-level ionization energies. These conditions can be generated at large-scale optical laser facilities such as the Laboratory for Laser Energetics (LLE)[40,42,44,45,47] or the National Ignition Facility (NIF),[58] in addition to being possible through direct, ultrafast x-ray stimulation at x-ray free-electron laser (XFEL) facilities such as the Free-Electron Laser in Hamburg (FLASH) and the Linac Coherent Light Source (LCLS).[59–63]

A first-principles theoretical treatment of NIXS for WDM must include a self-consistent determination of atomic potentials and ionization levels for a given range of state variables, while also being compatible with high densities and varying degrees of disorder in atomic positions. Our purpose here is to demonstrate an important step in the development of such a theoretical treatment. More specifically, we aim to calculate the valence-electron Compton profile in the impulse approximation using an extension of the real-space electronic structure and spectroscopy code FEFF.[64] This technique is quite appropriate for these studies since it does not require or depend on periodicity, and is thus applicable to aperiodic and disordered systems. However, we first present prototypical calculations and experimental results for cold, crystalline Be which serves as a well-characterized test case.[48,65–67] This application also serves as an anchoring reference system that validates and quantifies both our theoretical approach and implementation: Indeed, we demonstrate excellent agreement with experiment and with prior momentum-space methods designed for periodic structures. Similar agreement is found with experimental results for fcc Cu.

With this foundation, we can then consider applying the method to disordered and higher-temperature systems. Both the traditional condensed matter and the WDM communities have invested effort in understanding the thermal effects in NIXS. In the former, comparison of empirical modeling of thermal effects and experimental data up to ∼800 K (i.e., $k_BT \sim 0.07$ eV) shows that the dominant source of thermal effects on the Compton profile is indirect, arising from the thermally induced change of density of the simple metals investigated.[67,68] Thermally induced disorder is less important and the most direct thermal effect, smearing of the Fermi function or other reorganizations of the valence-electron wave functions, is negligible because of the metallic nature of the systems studied and the low temperatures relative to the structure in the unoccupied density of states. In the WDM context, on the other hand, density and more direct thermal effects play a more equal role. Existing methods for calculation of NIXS spectra in WDM treat the valence electrons as fully ionized and include only spherically averaged collisional effects from the ionic cores.[43,69–71] An improved theoretical treatment will, at a minimum, shed light on the accuracy of mean-field treatments, and may have a direct impact on ongoing studies of WDM in relevant geophysical and astrophysical conditions,[58,72] in inertial confinement fusion studies,[58] or in the unique nearly ordered WDM states that can be achieved with XFEL illumination.[59,62]

The remainder of this paper is organized as follows: In Sec. II, we survey the theoretical description of inelastic x-ray scattering. We then specialize to the high momentum-transfer regime in which the impulse approximation (IA) applies. It is in this regime that the NIXS spectrum is most clearly understood in terms of the Compton profile, which is directly related to the electronic momentum distribution. Here, we provide experimental data that illustrates the crossover from low momentum transfer, where collective excitations are visible, to high momentum transfer, where the spectrum is dominated by the Compton peak. Next, we detail how the electronic momentum density can be obtained from the real-space Green's function (RSGF) in the muffin-tin approximation. Section III contains details on the implementation of this theoretical framework. In Sec. IV, as a demonstration of the technique, we present detailed results for ordered Be metal and give a comparison with both experimental data and momentum-space Koringa-Kohn-Rostocker[73] (KKR) calculations. Although the real-space calculation is limited in momentum resolution by the size of the included cluster, we find very good agreement between real-space calculation, experimental data taken at a similar momentum resolution, and the broadened KKR calculation. We next compare the RSGF calculation of the valence Compton profile for Cu to experiment and prior KKR calculations, finding similarly good agreement. Next, in Sec. IV B, we compare theoretical RSGF calculations of NIXS spectra with experimental data taken at lower momentum transfer, where the IA no longer holds for the core electrons. In Sec. IV C, we briefly discuss the benefits of this approach compared to existing methods for treating NIXS from WDM. We then outline the steps we feel would be necessary to extend this work to these higher-temperature, disordered systems. Finally, Sec. V contains a summary and conclusions.

II. THEORY

A. Nonresonant inelastic x-ray scattering

In this paper, we consider an experiment in which a narrow-bandwidth beam of x rays is incident on a sample and the intensity of scattered radiation is measured as a function of energy and scattering angle. This two-photon process is described by a double-differential scattering cross section (DDSCS) $d^2\sigma/d\Omega d\omega_2(\mathbf{q},\omega)$, where Ω is the detected solid angle, ω_2 is the detected photon energy, and $\mathbf{q}$ and ω are the momentum and energy transferred to the sample in the scattering process. We will furthermore focus on the nonresonant inelastic x-ray scattering (NIXS) regime, in which the incident photon energy ω_1 is far from any electron binding energies in the sample. In this regime the dominant contribution to the DDSCS comes from the A^2 term in the interaction Hamiltonian at first order in perturbation theory. For $\hbar\omega$ well below the electron mass, where the nonrelativistic limit applies, the DDSCS is given by[74]

$$\frac{d^2\sigma}{d\Omega d\omega_2} = \left(\frac{d\sigma}{d\Omega}\right)_{\mathrm{Th}} S(\mathbf{q},\omega). \tag{1}$$

This has been factored into the probe-specific Thomson scattering cross section

$$\left(\frac{d\sigma}{d\Omega}\right)_{\mathrm{Th}} = \frac{\omega_2}{\omega_1} r_0^2 (\hat{\epsilon}_1 \cdot \hat{\epsilon}_2^*)^2 \tag{2}$$

and the sample-specific dynamic structure factor

$$S(\mathbf{q},\omega) = \sum_F \left| \langle F| \sum_j \exp(i\mathbf{q}\cdot\mathbf{r}_j)|I\rangle \right|^2 \delta(E_F - E_I - \hbar\omega). \tag{3}$$

Here, $r_0 = e^2/mc^2$ is the classical electron radius and $\hat{\epsilon}_{1,2}$ are incoming and outgoing photon polarizations. I and F are initial and final states of the sample, with energies E_I and E_F, respectively, and $\mathbf{r}_j$ is the position operator for the jth electron.

The physical information in the dynamic structure factor depends on the regime of $\mathbf{q}$ and ω. For example, by expanding the exponential transition operator, one sees that at low q, this reduces to a dipole operator. In this limit, the NIXS spectrum is very similar to an x-ray absorption spectrum, and thus contains information about the unoccupied density of states.[22,37] Here, we will instead be primarily interested in the regime of larger q and ω, in which the dynamic structure factor provides information about the ground-state electronic momentum density. This will be described in the following section.

First, however, to provide illustrative context, we present in Fig. 1 experimental NIXS data for polycrystalline Be taken at several different momentum transfers. We defer details of the experimental setup and data processing to Sec. IV B. Two sharp features are visible: the plasmon excitation at 25 eV and the Be K edge at 111.5 eV. Although very strong at low q, the collective plasmon peak quickly dies off as q is increased, indicating the onset of the single-particle excitation regime. Our focus in this paper will be on the broad Compton peak, which disperses and broadens as q is increased. This latter behavior is most easily understood in terms of the impulse approximation, to which we now turn.

B. Impulse approximation

For large energy transfer relative to the binding energy of an electron, and for large momentum transfer relative to the inverse electronic orbital size, Eisenberger and Platzman showed that, to a very good approximation, the NIXS from that electron can be described as Doppler-broadened Compton scattering.[75] In this approximation, known as the impulse approximation (IA), the single-electron potential before and after scattering cancels in the evaluation of the dynamic structure factor $S(\mathbf{q},\omega)$. The potential plays the simple role

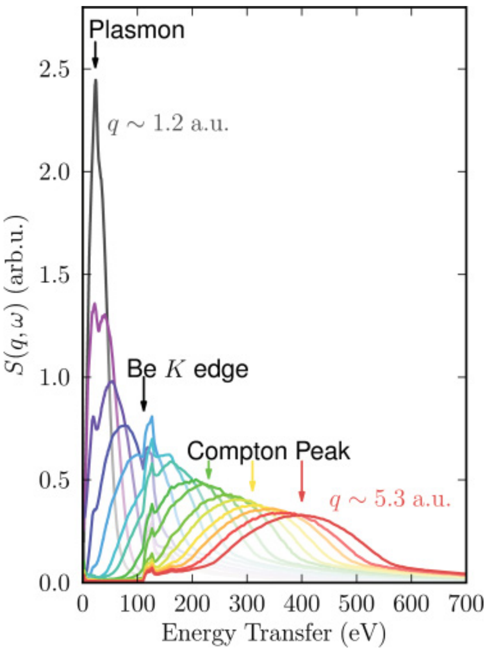

FIG. 1. (Color online) Experimental $S(q,\omega)$ for polycrystalline Be taken at 15 different fixed scattering angles. The average momentum transfer q for lowest and highest scattering angles is labeled. Features visible in the data are marked, including the collective plasmon excitation at smaller energy transfers, the Be K-absorption edge at 112 eV, and the Compton-scattering peak, which disperses with q.

of determining the momentum distribution of the electronic ground state, and consequently the shape of the Doppler broadened peak. In other words, the IA assumes that the photon-electron interaction occurs fast enough that the potential felt by the electron is identical before and after the interaction. Thus, energy conservation implies that

$$\hbar\omega = E_f - E_i = \frac{\hbar^2 q^2}{2m} + \frac{\hbar \mathbf{p}\cdot\mathbf{q}}{m}, \tag{4}$$

where $\mathbf{p}$ is the electron's momentum. This result is identical to that for classical Compton scattering of a photon from an electron with momentum $\mathbf{p}$. For fixed $\mathbf{q}$, the energy transfer is determined by the projection of the electron's momentum along the direction of the momentum transfer, $p_q \equiv \mathbf{p}\cdot\hat{\mathbf{q}}$, where $\hat{\mathbf{q}} = \mathbf{q}/|\mathbf{q}|$. The dynamic structure factor $S(\mathbf{q},\omega)$ must then be proportional to the number of electrons with a given value of this momentum projection. Indeed, one can show that in the IA,[75]

$$S(\mathbf{q},\omega) = (m/\hbar q)J(p_q), \tag{5}$$

$$J(p_q) \equiv \int d^3p\rho(\mathbf{p})\,\delta(p_q - (\omega m/q - \hbar q/2)), \tag{6}$$

where $\rho(\mathbf{p})$ is the one-particle electronic momentum density. $J(p_q)$, commonly referred to as the Compton profile (CP), gives precisely the average number of electrons with momentum-projection p_q. From Eqs. (4)–(6), we see that the resulting Compton peak in the NIXS spectrum will be centered around $\omega = \hbar q^2/2m$ and have a width proportional to both the width of the one-electron momentum distribution and the momentum transfer. This explains the dispersion and broadening visible in Fig. 1.

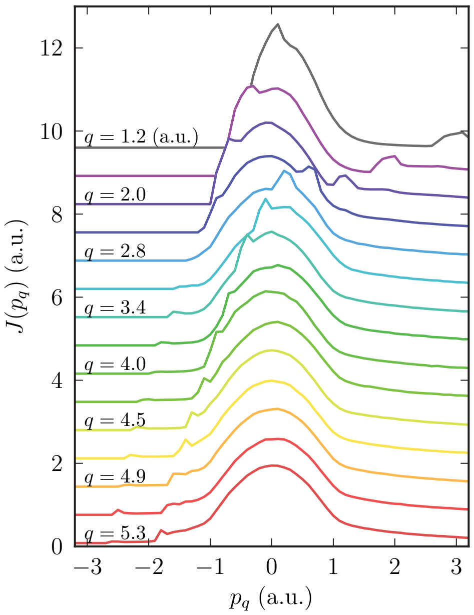

FIG. 2. (Color online) The same data as Fig. 1 after changing variables to $J(p_q)$. All momentum transfers q are in a.u. Above the Be K-absorption edge, the spectra are nearly identical, showing the applicability of the impulse approximation in that regime. The sharp feature dispersing across the Compton peak for intermediate q is the Be K edge. The plasmon excitation peak is visible in the four curves with lowest q.

In the independent-particle approximation, $S(\mathbf{q},\omega)$ can be written as a sum over independent, noninterfering contributions from valence, semicore, and core electrons. Thus, the respective contributions to the CP can also be separated. For the valence contribution, the conditions of the IA are satisfied for all but the lowest q. On the other hand, for the core contribution, only the high-energy-transfer tail is correctly described by the IA. In Fig. 2, we show the Be NIXS spectra after switching variables from $S(\mathbf{q},\omega)$ to $J(p_q)$. The Compton peak is centered about $p_q = 0$, consistent with vanishing average electron momentum. The valence contribution is sharper, extending between ≈±1 a.u. The core contribution is broader, extending well above +3 a.u., with a low-energy-transfer cutoff that is q dependent. This cutoff occurs when the energy transfer is equal to the K-shell binding energy, and thus disperses from −2 to +3 a.u. as q decreases from 5.3 to 1.2 a.u. Additionally, the plasmon peak is seen at small negative p_q for the lowest values of momentum transfer. It is clear that once well above the K-absorption edge, the spectra are nearly identical, indicating the validity of the IA.

C. Real-space formalism for valence Compton profile

If the IA holds, then, as seen in Eq. (6), the dominant ingredient required for calculation of the Compton profile is the one-electron momentum density $\rho(\mathbf{p})$. Several techniques exist to calculate $\rho(\mathbf{p})$. Existing methods for solids typically use a band-structure approach, and thus impose a requirement of periodic structure,[74] complicating the application to disordered systems. Some classes of disorder, such as substitutionally disordered alloys, have been treated in KKR calculations by using the coherent potential approximation, in which the alloy is replaced by an ordered system with a single averaged effective site potential.[76] An early attempt at describing thermal effects in Li was based on calculating band structures for frozen configurations in eight-atom supercells.[77] These calculations predicted a broadening of the CP with increased temperature. In contrast, subsequent experiments on Al, Li, and Be found instead that the CP became narrower as temperature increased.[67,68] By comparing to a pseudopotential model that included thermal effects by scaling the plane-wave components by Debye-Waller factors, these authors attributed the dominant source of the effect to be from thermal expansion of the lattice. We seek to relax the constraint of periodicity by using a real-space analog of KKR, as implemented in the FEFF code,[64] to calculate the Green's function in the muffin-tin approximation for an arbitrary cluster of atomic sites. This code builds in self-consistent potentials, quasiparticle effects, relativistic effects, and disorder and has been widely used for calculations of core-level x-ray spectroscopy. However, the extension of FEFF to the valence regime as discussed here is still developmental.[78]

Briefly the strategy of the code is as follows: Given the locations and species of atoms in a cluster, FEFF calculates atomic wave functions for each unique species using a Dirac-Hartree-Fock solver. Next, the atomic densities and cluster structure are used to form overlapped atomic potentials in the spherical muffin-tin approximation. The real-space one-particle Green's function is then constructed, including the full effects of multiple scattering from other atoms within a specified radius. The density of states (DOS) is calculated by integrating the imaginary part of the Green's function over all space (as approximated by a sum over Norman spheres centered at each site[79]). The Fermi level is determined by integrating the DOS to give the appropriate number of electrons. The density is then recalculated from the Green's function, giving updated potentials. This process is iterated until self-consistent.

The momentum-space density $\rho(\mathbf{p})$ is related to the real-space density matrix $\rho(\mathbf{r},\mathbf{r}')$ via a Fourier transform:

$$\rho(\mathbf{p}) = \int d^3r\, d^3r'\, e^{i\mathbf{p}\cdot(\mathbf{r}-\mathbf{r}')}\rho(\mathbf{r},\mathbf{r}'). \tag{7}$$

Choosing the z axis to lie along $\hat{\mathbf{q}}$, combining Eqs. (6) and (7), and integrating over p_x and p_y gives delta functions that set $x = x'$ and $y = y'$. After performing the x' and y' integrals we have

$$J(p_q) = \int dx\, dy\, dz\, dz'\, e^{ip_q(z-z')}\rho(\mathbf{r},\mathbf{r}'), \tag{8}$$

where $\mathbf{r} = (x,y,z)$ and $\mathbf{r}' = (x,y,z')$.

Now, the real-space density matrix is related to Green's function by

$$\rho(\mathbf{r},\mathbf{r}') = -\frac{2}{\pi}\mathrm{Im}\int_{E_c}^{\infty} dE\, G(\mathbf{r},\mathbf{r}',E) f_T(E), \tag{9}$$

where $f_T(E) = 1/(e^{(E-\mu)/k_BT} + 1)$ is the Fermi distribution and μ is the chemical potential. For our purposes, we are interested in the valence CP, so the lower-energy cutoff E_c is set in the gap between core and valence states (typically around -30 eV). In this paper, all calculations are at $T = 0$, so the Fermi distribution is replaced by $\Theta(E_F - E)$, where E_F is the Fermi energy. The factor of 2 comes from spin degeneracy (here we assume no spin dependence in G, although it is straightforward to generalize).

Finally, the Green's function can be expressed in the muffin-tin approximation as[78]

$$G(\mathbf{r},\mathbf{r}',E) = -2k\Bigg[\delta_{n,n'}\sum_L H^E_{Ln}(\mathbf{r}_>)\bar{R}^E_{Ln'}(\mathbf{r}_<) + \sum_{L,L'} R^E_{Ln}(\mathbf{r}_n)e^{i\delta_{Ln}}\, g^E_{Ln,L'n'}\, e^{i\delta_{L'n'}}\, \bar{R}^E_{L'n'}(\mathbf{r}'_{n'})\Bigg]. \tag{10}$$

The indices n and n' label the atomic sites nearest $\mathbf{r}$ and $\mathbf{r}'$, and $\mathbf{r}_n \equiv \mathbf{r} - \mathbf{R}_n$, where $\mathbf{r}_n$ is the center of the nth site. $R^E_{Ln}(\mathbf{r}) = i^l R^E_{Ln}(r)Y_L(\hat{r})$ is the regular solution at site n with angular momentum L and energy E. $H^E = N^E - iR^E$, where N^E is the irregular solution. The overbar denotes complex conjugation of all parts except for the radial function, e.g., $\bar{R}^E_{Ln}(\mathbf{r}) = (-i)^l R^E_{Ln}(r)Y^*_L(\hat{r})$. δ_{Ln} gives the scattering phase shift and $g^E_{Ln,L'n'}$ is the full multiple-scattering (FMS) matrix.[80] For a derivation of Eq. (10), we refer to the Appendix of Prange *et al.*[78] and references therein.

D. Core contribution

The IA does not hold for the core contribution to $S(\mathbf{q},\omega)$ at the momentum transfers shown in Figs. 1 and 2 since the energy transfer is comparable to the core binding energy. In this case, it is possible to calculate the core NIXS contribution directly using the RSGF approach described by Soininen *et al.*[23] We give results using this approach below, in Sec. IV B.

At higher momentum transfer (as would be accessible with higher incident photon energy), or when only interested in the high-energy-transfer portion of the spectrum, it is possible to use the IA for the core contribution. Since solid-state effects on the localized core wave function are typically negligible, the core momentum density can be obtained directly from Fourier-transformed atomic Hartree-Fock wave functions using $\rho(p) = \sum_i |\phi(p)|^2$. The core CP in the IA can then be obtained by combining this with Eq. (6).

III. COMPUTATIONAL DETAILS

We have extended FEFF to calculate the momentum density $\rho(p)$ in Eq. (7) and thence the Compton profile. Our procedure makes use of a subroutine RHORRP in FEFF, which calculates the density matrix $\rho(\mathbf{r},\mathbf{r}')$ by combining Eqs. (9) and (10). To calculate the CP from Eq. (8), we approximate the integral over $\mathbf{r}$ as a sum over Norman spheres centered at each atomic site. For a given term in this sum, $\mathbf{r}$ is constrained to lie within the Norman radius while z' is allowed to vary over all space (in practice, limited by the size of the cluster). In a periodic system with a monatomic unit cell each site is identical, so the integral need only be performed for a single site. This normalizes the integral of the resulting CP to the number of valence electrons per atom. In general, $\mathbf{r}$ must be integrated over each unique site

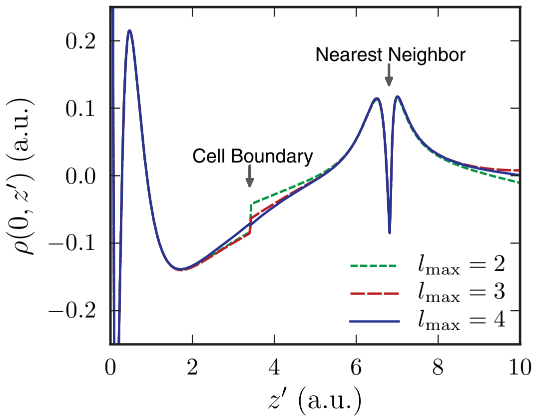

FIG. 3. (Color online) Dependence of Cu density matrix on angular momentum cutoff $l_{\max}$. A slice of $\rho(r,r')$ with r fixed near the origin and r' varying along the z axis is shown. The discontinuity at $\sim$3.4 a.u. occurs as r' moves from one cell into another. As $l_{\max}$ is increased, the discontinuity decreases.

in the system, e.g., every site in the cluster for a completely disordered system.

The sum over angular momenta in Eq. (10) is truncated at a configurable upper bound $l_{\max}$. Since the size of the FMS matrix $g^E_{Ln,L'n'}$ scales as $(l_{\max}+1)^4$, it is desirable to keep this bound as low as possible. However, if the value used is too low, the density matrix becomes inaccurate away from the center of a site, leading to a discontinuity as z' moves from one site to another. In Fig. 3, we show a slice of the density matrix $\rho(\mathbf{r},\mathbf{r}')$ with $\mathbf{r}$ fixed near the origin and $\mathbf{r}'$ varying along the $\hat{z}$ axis. The discontinuity at the point marked "Cell Boundary" is clear for small $l_{\max}$ and decreases as $l_{\max}$ is increased. Typically the discontinuity is negligible for $l_{\max} \geqslant l_{\mathrm{v}}$, where l_{v} is the atomic valence orbital angular momentum (e.g., $l_{\max} = 4$ for transition metals).

Numerical integration of Eq. (6) is performed in cylindrical coordinates. At each z,z' point, the integral over the x-y plane is calculated. This reduced $\rho(z,z')$ is then Fourier transformed to obtain the CP. In some cases, the CP calculated in this fashion displays oscillatory aliasing effects from the finite range of the Fourier transform. A Hann apodization function can be included to remove these. The finite range of z' has two further consequences. First, some momentum density is missed, resulting in the integral of the CP being less than the number of valence electrons per atom. This $\lesssim$5% effect is corrected for by rescaling the CP. Second, the CP is broadened due to the convolution theorem, reducing the momentum resolution to $\sim\pi/z'_{\max}$. This latter factor is one key limitation of this technique: The number of atoms in a cluster scales as the cube of the radius, placing a practical bound on the attainable momentum resolution.

IV. RESULTS AND DISCUSSION

A. Valence Compton profile

In order to validate our framework, we have calculated the valence Compton profile (CP) for Be at ambient conditions with lattice constants $a = 4.3289$ a.u. and $c = 6.7675$ a.u. These calculations are compared to experimental data and momentum-space (KKR) theoretical calculations from Huotari *et al.*[65] Comparisons are made for the three main crystallographic directions of the hexagonal-close-packed structure ([100], [110], and [001], where the $\hat{a}$ and $\hat{b}$ basis vectors have been chosen to be 60° apart). In Fig. 4 we present the primary result of this paper, showing very good agreement between the present real-space theory and momentum-space theory, and good agreement between both theories and experiment. We now give contextual details for the comparison.

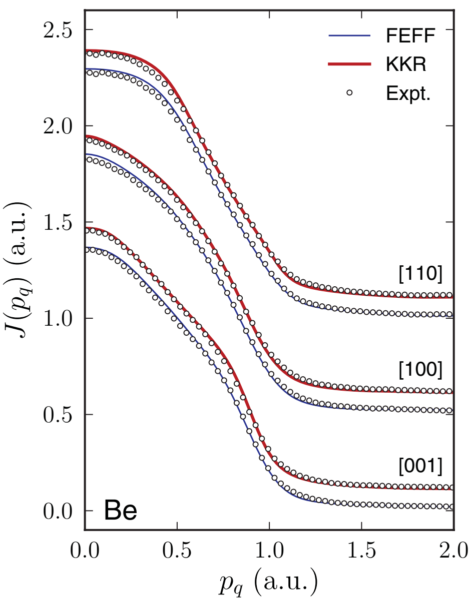

FIG. 4. (Color online) Be Compton profile. Experimental data from Huotari *et al.* (Ref. 65) is compared to a momentum-space (KKR) calculation from the same reference and our real-space (FEFF) calculation. The experimental data were taken at 56 keV and have had the theoretical core contribution and a small linear background subtracted. For each direction, the same experimental data is presented twice (once for each theory). The experimental statistical uncertainty is smaller than the symbol size. The Fermi surface is located at the inflection point of the CP, just below 1 a.u.

The experimental data in Fig. 4 (reproduced from Huotari *et al.*[65]) were taken at 56 keV with a momentum resolution of 0.16 a.u. The momentum-space theoretical calculations (also from Huotari *et al.*[65]) were performed using the KKR (Ref. 73) methodology. Crystal potentials were calculated in the local density approximation (LDA), and exchange and correlation effects were approximated via the isotropic Lam-Platzman (LP) correction.[81]

Our real-space calculations were performed using a cluster of 522 atoms within a sphere of 10-Å radius with $l_{\max} = 2$. Increasing $l_{\max}$ beyond this value had no effect for this low-z material. The density matrix was evaluated with $\mathbf{r}$ on a $32 \times 32 \times 32$ point cylindrical grid and z' at 144 points between ±30 a.u. The range over which z' is integrated is limited by the cluster size. This limits the momentum resolution of the real-space theoretical CP to $\delta q = \pi/30 \simeq 0.1$ a.u. Lattice motion, which can be approximately treated by FEFF, has been neglected. The LP correction has not been applied to the real-space calculations.

As described by Huotari *et al.*,[65] a linear background has been subtracted from the experimental data. Additionally,

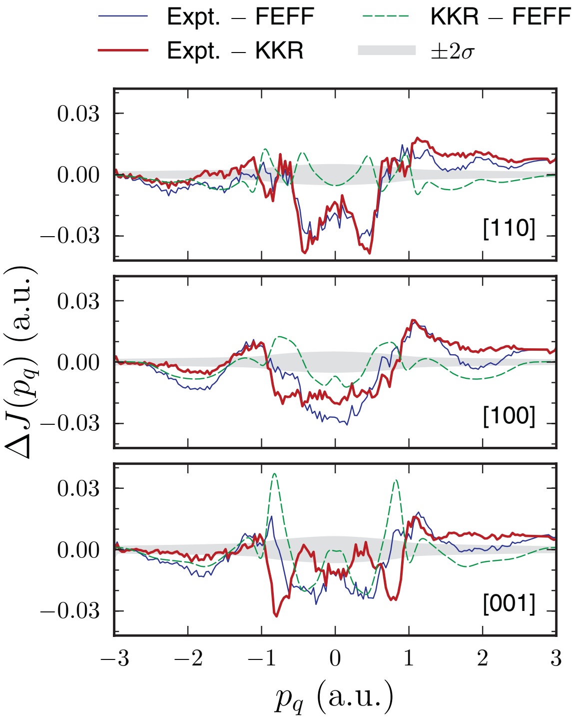

FIG. 5. (Color online) Be Compton profile differences. The solid curves show the difference between experiment and theory. The dashed curve is the difference between theories. These are superimposed on the $\pm 2\sigma$ range of experimental statistical uncertainty.

since it is our purpose to compare valence profile calculations, we have subtracted the theoretical core profile presented in the original reference.[65] The theoretical curves in Fig. 4 are offset for clarity, and for each direction the same experimental data is presented twice (once for each theory). Absolute differences between these curves are shown in Fig. 5. The two theories are in similarly good agreement with experiment. Significant systematic errors are introduced by the subtraction of the core CP, which most likely is the cause of the linear trend in the differences with experiment. The FEFF calculations slightly overestimate the momentum density in the range $1 < |p_q| < 2$. It is unclear whether this is a numerical artifact or a consequence of the muffin-tin approximation. The largest discrepancy between the two theories is at $|p_q| \sim 0.9$ in the [001] direction, and is below the 5% level. Given the analogous nature of the KKR and RSGF methods, one would expect the two theoretical results to differ by the LP correction, which was only applied to the KKR theory. This discrepancy may be due to differing muffin-tin radii. The KKR calculation assumes nonoverlapping muffin tins, while the RSGF calculation uses overlapping muffin tins.[64] As pointed out in Huotari *et al.*,[65] the residuals with experiment are similar in shape to the LP correction, suggesting that were it included in the RSGF calculation, the agreement would be even better. Finally, in order to more clearly see the fine structure, we show the derivative of the CP in Fig. 6. Here, the experimental data were numerically differentiated using a three-point derivative, with no additional smoothing. The overall similarity between the two theoretical curves further validates our implementation of the RSGF technique.

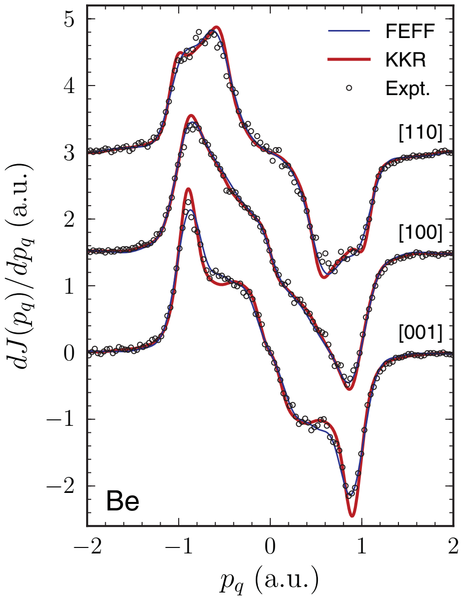

FIG. 6. (Color online) Be Compton profile derivative. The same experimental data and theoretical calculations as Fig. 4 are shown, but this time as first derivatives. The fine structure of the profile is more clearly seen here. Experimental statistical uncertainty is smaller than the symbol size. The Fermi surface is located at the extrema of the derivative.

Given the good agreement with Be, it is natural to ask if the RSGF method extends to other simple metals that are well described in the muffin-tin approximation. We have included a calculation of the valence CP for crystalline Cu with $\hat{q}$ along the [110] direction. In Fig. 7, we compare the FEFF calculation with KKR and with two different experiments. The KKR calculation and experiment labeled Sakurai are reproduced from Sakurai *et al.*[82] The experimental data was taken using 59.38-keV x rays with a momentum resolution of 0.12 a.u. Additionally, we include a γ-ray measurement (412 keV incident, 0.41 a.u. momentum resolution) from Pattison *et al.*[83] The FEFF calculations were performed using a cluster of 176 atoms within a sphere of 8-Å radius with $l_{\max} = 4$. The density matrix was evaluated with $\mathbf{r}$ on a $48 \times 48 \times 48$ point cylindrical grid and z' at 256 points between ± 20 a.u. Again, the FEFF and KKR calculations are similar. Even after accounting for momentum resolution, the two experiments are not in agreement with each other. This disagreement has been attributed to systematic errors introduced while correcting for multiple Compton-scattering events.[82] These errors are expected to be smaller in the Sakurai dataset, but the agreement between theory and the supposedly erroneous Pattison dataset is impressive, and suggest that a reinterpretation of the experimental data may be appropriate.

B. Comparison of FEFF with NIXS data

In the prior section, we have focused on experimental data taken for the explicit purpose of studying the CP, and thus taken well into the regime of applicability of the IA. Often, as in NIXS studies of WDM, the energy- and momentum-transfer regimes accessible are more intermediate. The IA typically

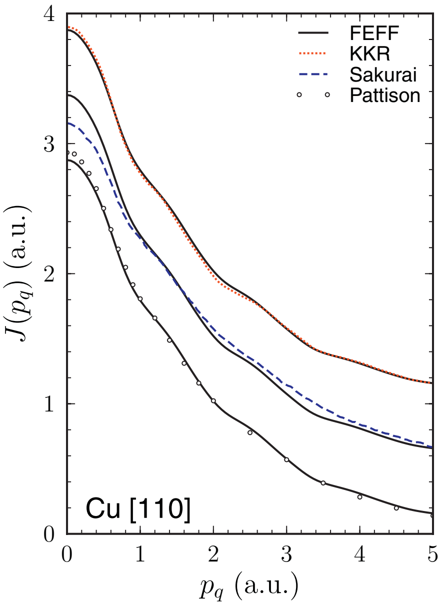

FIG. 7. (Color online) Cu [110] valence Compton profile. Curves have been offset by 0.5 a.u. for clarity. The KKR calculation and x-ray scattering data (59.38 keV incident, 0.12 a.u. momentum resolution) from Sakurai *et al.* (Ref. 82). For comparison we have included a γ-ray dataset (412 keV incident, 0.41 a.u. momentum resolution) from Pattison *et al.* (Ref. 83).

does not apply to scattering from the core electrons, and at lower momentum transfer breaks down even for the valence electrons. Our purpose in this section is to find the limits of applicability of the RSGF technique in this intermediate regime.

Experimental data in this section (also presented in Figs. 1 and 2) were collected using the recently upgraded LERIX instrument at beamline 20-ID at the Advanced Photon Source.[6,84] The instrument consists of 19 spherically bent Si crystal analyzers on a 1-m radius semicircle. The incident beam is polarized normal to the plane of the semicircle, so the polarization factor from Eq. (2) is unity for all analyzers. Each analyzer selects a narrow band of radiation around 9890 eV at a fixed scattering angle. The incident beam energy is varied to cover the energy-loss region of interest. The energy-loss scale is independently calibrated to within 0.1 eV for each analyzer using the center of the elastic scattering peak and points within each spectrum are normalized to the incident flux measured by an ion chamber upstream of the sample.

For fixed scattering angle θ, the magnitude of q is given by

$$q^2 = \omega_1^2 + \omega_2^2 - 2\omega_1\omega_2\cos(\theta). \tag{11}$$

Combining this with Eq. (6), it is straightforward to convert from the valence CP to $S(\theta,\omega)$. Since the IA does not apply for the core, we use the FEFFQ package[23] to calculate the directionally averaged core contribution to $S(q,\omega)$. This is done for a fine mesh of q values, which are interpolated between using Eq. (11) to obtain the fixed-angle $S(\theta,\omega)$.

We have subtracted a small linear background from the data. Although it is possible to apply f-sum normalization to $S(q,\omega)$, the same is not true for $S(\theta,\omega)$. For this reason, the overall normalization of the data was left as a free parameter.

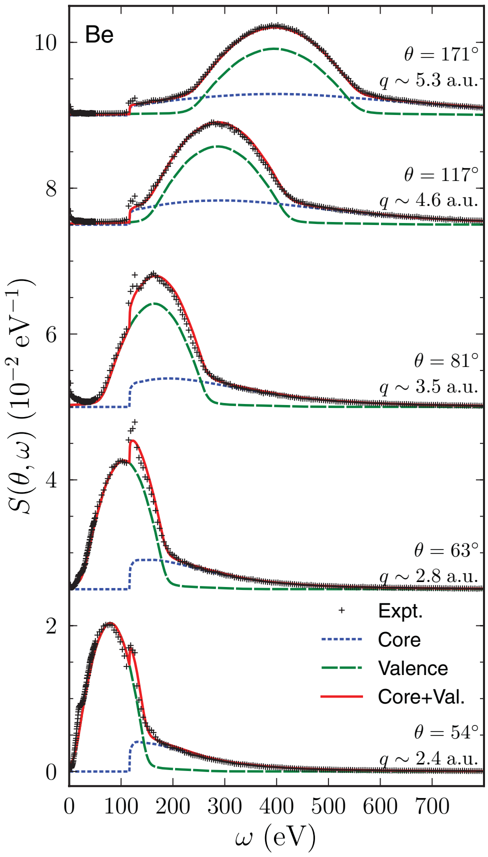

FIG. 8. (Color online) Comparison with NIXS data for polycrystalline Be at five different values of momentum transfer q. The core contribution to the spectrum is calculated using FEFFQ package (Ref. 23). The valence is calculated using the techniques described in this paper and averaged over the three main crystallographic directions. At the lowest two values of momentum transfer, a plasmon excitation is visible at ~25 eV. This signals the onset of the collective regime and the breakdown of the IA for the valence electrons.

The results for several different scattering angles are shown in Fig. 8. Close to backscatter ($\theta \gtrsim 110°$), the agreement is very good. In our calculations of the core contribution, this detailed near-edge structure (XANES) was not included, leading to the noticeable differences at the Be K edge. As q is decreased, the IA becomes less valid and some discrepancies emerge. Additionally, the collective plasmon excitation is present in the experimental data for the lowest q value shown (at $\omega \sim 20$), which is not modeled in the RSGF theory.

C. Application to WDM

Before concluding, we recall that a long-term goal of this paper is to extend its application to high temperature and/or disordered systems, as in the case of WDM. Present methods for treating NIXS from WDM calculate the valence-electron contribution to the dynamic structure factor within the random phase approximation (RPA) from the dielectric function using the fluctuation-dissipation theorem.[43,69–71] The valence electrons are treated as free, with effects of collisions with ionic cores included perturbatively in the Born-Mermin approximation (BMA).[71] At lower densities, collisions are infrequent and the BMA approach is unlikely to omit quantitatively important aspects of the behavior of unbound electrons. However, at solidlike and higher densities, any perturbative treatment of the dominant physical presence in the system, the ionic cores, will clearly benefit from independent validation against more complete theoretical treatments. By contrast, the approach present in this paper includes all orders of valence-electron scattering caused by such condensed phase effects.

The most complete extension of the RSGF approach to calculations of WDM phases will require several steps beyond the present paper. First, thermal and static structural disorder can be treated approximately by including Debye-Waller factors in the FMS calculation.[80] More general structural disorder can be treated by averaging over configurations taken from finite-temperature, molecular dynamics simulations. These disorder effects tend to dampen the fine structure in the density function. Second, the smearing of the Fermi distribution can be handled as in Eq. (9); the Fermi function should be included self-consistently in the calculation of the Green's function and density matrix. Finally, for the WDM case with temperatures comparable to or larger than the Fermi energy, a more appropriate, finite-temperature exchange-correlation potential is called for, which will likely affect the width of the Compton profile.

V. CONCLUSIONS

We have demonstrated a real-space Green's function technique for calculating valence Compton profiles for Be and Cu. We find close agreement with high momentum-transfer experimental measurements and prior theoretical calculations for these systems, validating the implementation. Furthermore, we have shown that the technique can be used at moderate momentum transfer as long as the core contribution to the dynamic structure factor is properly treated. Although periodic systems were chosen for the comparison, the technique does not require periodicity and thus should be readily applicable to disordered systems. This lays the groundwork for first-principles calculations of high momentum-transfer NIXS from WDM, where disorder in potentials, ionization, and atomic structure is expected to be relevant.

ACKNOWLEDGMENTS

This work is supported by the US Department of Energy, Basic Energy Sciences, Grants No. DE-SC0002194 (B.A.M., G.T.S., J.I.P.) and No. DE-FG03-97ER45623 (J.J.R., J.J.K.). We thank S. Huotari and A. Bansil for graciously providing us with both experimental data and prior theoretical calculations in a numerical form, and also thank C. Fortmann, T. Döppner, and J. Bradley for many enlightening discussions. PNC/XSD facilities at the Advanced Photon Source, and research at these facilities, are supported by the US Department of Energy - Basic Energy Sciences, a Major Resources Support grant from NSERC, the University of Washington, Simon Fraser University and the Advanced Photon Source. Use of the Advanced Photon Source, an Office of Science User Facility operated for the U.S. Department of Energy (DOE) Office of Science by Argonne National Laboratory, was supported by the U.S. DOE under Contract No. DE-AC02-06CH11357.

---

[*] seidler@uw.edu

[1] S. Doniach, P. M. Platzman, and J. T. Yue, Phys. Rev. B **4**, 3345 (1971).

[2] A. H. Compton, Phys. Rev. **21**, 483 (1923).

[3] J. W. M. Dumond, Science **9**, 452 (1928).

[4] P. Suortti, T. Buslaps, P. Fajardo, V. Honkimäki, M. Kretzschmer, U. Lienert, J. E. McCarthy, M. Renier, A. Shukla, Th. Tschentscher, and T. Meinander, J. Synchrotron Radiat. **6**, 69 (1999).

[5] Y. Sakurai, M. Ito, T. Urai, Y. Tanaka, N. Sakai, T. Iwazumi, H. Kawata, M. Ando, and N. Shiotani, Rev. Sci. Instrum. **63**, 1190 (1992).

[6] T. T. Fister, G. T. Seidler, L. Wharton, A. R. Battle, T. B. Ellis, J. O. Cross, A. T. Macrander, W. T. Elam, T. A. Tyson, and Q. Qian, Rev. Sci. Instrum. **77**, 063901 (2006).

[7] R. Verbeni, T. Pylkkänen, S. Huotari, L. Simonelli, G. Vankó, K. Martel, C. Henriquet, and G. Monaco, J. Synchrotron Radiat. **16**, 469 (2009).

[8] Y. Sakurai, M. Itou, B. Barbiellini, P. E. Mijnarends, R. S. Markiewicz, S. Kaprzyk, J. M. Gillet, S. Wakimoto, M. Fujita, S. Basak, Y. J. Wang, W. Al-Sawai, H. Lin, A. Bansil, and K. Yamada, Science **332**, 698 (2011).

[9] B. Barbiellini, A. Koizumi, P. E. Mijnarends, W. A. Sawai, H. Lin, T. Nagao, K. Hirota, M. Itou, Y. Sakurai, and A. Bansil, Phys. Rev. Lett. **102**, 206402 (2009).

[10] B. Barbiellini, Ch, G. Loupias, T. Buslaps, and A. Shukla, Phys. Rev. B **79**, 155115 (2009).

[11] M. Hakala, K. Nygaard, S. Manninen, S. Huotari, T. Buslaps, A. Nilsson, L. G. M. Pettersson, and K. Hämäläinen, J. Chem. Phys. **125**, 084504 (2006).

[12] M. Hakala, K. Nygaard, J. Vaara, M. Itou, Y. Sakurai, and K. Hämäläinen, J. Chem. Phys. **130**, 034506 (2009).

[13] J. T. Okada, P. H.-L. Sit, Y. Watanabe, Y. J. Wang, B. Barbiellini, T. Ishikawa, M. Itou, Y. Sakurai, A. Bansil, R. Ishikawa, M. Hamaishi, T. Masaki, P.-F. Paradis, K. Kimura, T. Ishikawa, S. Nanao, Phys. Rev. Lett. **108**, 067402 (2012)

[14] I. Juurinen, K. Nakahara, N. Ando, T. Nishiumi, H. Seta, N. Yoshida, T. Morinaga, M. Itou, T. Ninomiya, Y. Sakurai, E. Salonen, K. Nordlund, K. Hämäläinen, and M. Hakala, Phys. Rev. Lett. **107**, 197401 (2011).

[15] J. A. Bradley, G. T. Seidler, G. Cooper, M. Vos, A. P. Hitchcock, A. P. Sorini, C. Schlimmer, and K. P. Nagle, Phys. Rev. Lett. **105**, 053202 (2010).

[16] J. A. Bradley, S. S. Gupta, G. T. Seidler, K. T. Moore, M. W. Haverkort, G. A. Sawatzky, S. D. Conradson, D. L. Clark, S. A. Kozimor, and K. S. Boland, Phys. Rev. B **81**, 193104 (2010).

[17] J. A. Bradley, P. Yang, E. R. Batista, K. S. Boland, C. J. Burns, D. L. Clark, S. D. Conradson, S. A. Kozimor, R. L. Martin, G. T. Seidler, B. L. Scott, D. K. Shuh, T. Tyliszczak, M. P. Wilkerson, and L. E. Wolfsberg, J. Am. Chem. Soc. **132**, 13914 (2010).

[18] Y. Feng, J. A. Soininen, A. L. Ankudinov, J. O. Cross, G. T. Seidler, A. T. Macrander, J. J. Rehr, and E. L. Shirley, Phys. Rev. B **77**, 165202 (2008).

[19]T. T. Fister, D. D. Fong, J. A. Eastman, H. Iddir, P. Zapol, P. H. Fuoss, M. Balasubramanian, R. A. Gordon, K. R. Balasubramaniam, and P. A. Salvador, Phys. Rev. Lett. **106**, 037401 (2011).

[20]T. T. Fister, F. D. Vila, G. T. Seidler, L. Svec, J. C. Linehan, and J. O. Cross, J. Am. Chem. Soc. **130**, 925 (2007).

[21]R. A. Gordon, G. T. Seidler, T. T. Fister, and K. P. Nagle, J. Electron Spectrosc. Relat. Phenom. **184**, 220 (2011).

[22]W. Schűlke, *Electron Dynamics by Inelastic X-Ray Scattering*, Oxford Series on Synchrotron Radiation (Oxford University Press, New York, 2007).

[23]J. A. Soininen, A. L. Ankudinov, and J. J. Rehr, Phys. Rev. B **72**, 045136 (2005).

[24]U. Bergmann, A. Di Cicco, P. Wernet, E. Principi, P. Glatzel, and A. Nilsson, J. Chem. Phys. **127**, 174504 (2007).

[25]I. Waluyo, D. Nordlund, U. Bergmann, L. G. M. Pettersson, and A. Nilsson, J. Chem. Phys. **131**, 031103 (2009).

[26]I. Waluyo, C. Huang, D. Nordlund, U. Bergmann, T. M. Weiss, L. G. M. Pettersson, and A. Nilsson, J. Chem. Phys. **134**, 064513 (2011).

[27]H. Conrad, F. Lehmkühler, C. Sternemann, A. Sakko, D. Paschek, L. Simonelli, S. Huotari, O. Feroughi, M. Tolan, and K. Hämäläinen, Phys. Rev. Lett. **103**, 218301 (2009).

[28]O. M. Feroughi, C. Sternemann, Ch. J. Sahle, M. A. Schroer, H. Sternemann, H. Conrad, A. Hohl, G. T. Seidler, J. Bradley, T. T. Fister, M. Balasubramanian, A. Sakko, K. Pirkkalainen, K. Hämäläinen, and M. Tolan, Appl. Phys. Lett. **96**, 081912 (2010).

[29]M. W. Haverkort, A. Tanaka, L. H. Tjeng, and G. A. Sawatzky, Phys. Rev. Lett. **99**, 257401 (2007).

[30]S. S. Gupta, J. A. Bradley, M. W. Haverkort, G. T. Seidler, A. Tanaka, and G. A. Sawatzky, Phys. Rev. B **84**, 075134 (2011).

[31]K. Hämäläinen, S. Galambosi, J. A. Soininen, E. L. Shirley, J. P. Rueff, and A. Shukla, Phys. Rev. B **65**, 155111 (2002).

[32]M. H. Krisch, F. Sette, C. Masciovecchio, and R. Verbeni, Phys. Rev. Lett. **78**, 2843 (1997).

[33]T. T. Fister, M. Schmidt, P. Fenter, C. S. Johnson, M. D. Slater, M. K. Y. Chan, and E. L. Shirley, J. Chem. Phys. **135**, 224513 (2011).

[34]W. A. Caliebe, J. A. Soininen, E. L. Shirley, C. C. Kao, and K. Hämäläinen, Phys. Rev. Lett. **84**, 3907 (2000).

[35]J. A. Soininen, K. Hämäläinen, W. A. Caliebe, C. C. Kao, and E. L. Shirley, J. Phys.: Condens. Matter **13**, 8039 (2001).

[36]M. Balasubramanian, C. S. Johnson, J. O. Cross, G. T. Seidler, T. T. Fister, E. A. Stern, C. Hamner, and S. O. Mariager, Appl. Phys. Lett. **91**, 031904 (2007).

[37]U. Bergmann, P. Glatzel, and S. P. Cramer, Microchem. J. **71**, 221 (2002).

[38]U. Bergmann, Ph, P. Glatzel, M. Cavalleri, L. G. M. Pettersson, A. Nilsson, and S. P. Cramer, Phys. Rev. B **66**, 092107 (2002).

[39]Y. Feng, G. T. Seidler, J. O. Cross, A. T. Macrander, and J. J. Rehr, Phys. Rev. B **69**, 125402 (2004).

[40]T. Döppner, O. L. Landen, H. J. Lee, P. Neumayer, S. P. Regan, and S. H. Glenzer, High Energy Density Phys. **5**, 182 (2009).

[41]R. R. Fäustlin, Th, T. Döppner, S. Düsterer, E. Förster, C. Fortmann, S. H. Glenzer, S. Göde, G. Gregori, R. Irsig, T. Laarmann, H. J. Lee, B. Li, K. H. M. Broer, J. Mithen, B. Nagler, A. Przystawik, H. Redlin, R. Redmer, H. Reinholz, G. Röpke, F. Tavella, R. Thiele, J. Tiggesbäumker, S. Toleikis, I. Uschmann, S. M. Vinko, T. Whitcher, U. Zastrau, B. Ziaja, and Th. Tschentscher, Phys. Rev. Lett. **104**, 125002 (2010).

[42]S. H. Glenzer, G. Gregori, F. J. Rogers, D. H. Froula, S. W. Pollaine, R. S. Wallace, and O. L. Landen, Phys. Plasmas **10**, 2433 (2003).

[43]S. H. Glenzer and R. Redmer, Rev. Mod. Phys. **81**, 1625 (2009).

[44]S. H. Glenzer, G. Gregori, R. W. Lee, F. J. Rogers, S. W. Pollaine, and O. L. Landen, Phys. Rev. Lett. **90**, 175002 (2003).

[45]S. H. Glenzer, H. J. Lee, P. Davis, T. Döppner, R. W. Falcone, C. Fortmann, B. A. Hammel, A. L. Kritcher, O. L. Landen, and R. W. Lee, High Energy Density Phys. **6**, 1 (2010).

[46]A. L. Kritcher, P. Neumayer, J. Castor, T. Döppner, R. W. Falcone, O. L. Landen, H. J. Lee, R. W. Lee, E. C. Morse, A. Ng, S. Pollaine, D. Price, and S. H. Glenzer, Science **322**, 69 (2008).

[47]S. H. Glenzer, O. L. Landen, P. Neumayer, R. W. Lee, K. Widmann, S. W. Pollaine, R. J. Wallace, G. Gregori, A. Höll, T. Bornath, R. Thiele, V. Schwarz, W. D. Kraeft, and R. Redmer, Phys. Rev. Lett. **98**, 065002 (2007).

[48]H. J. Lee, P. Neumayer, J. Castor, T. Döppner, R. W. Falcone, C. Fortmann, B. A. Hammel, A. L. Kritcher, O. L. Landen, R. W. Lee, D. D. Meyerhofer, D. H. Munro, R. Redmer, S. P. Regan, S. Weber, and S. H. Glenzer, Phys. Rev. Lett. **102**, 115001 (2009).

[49]E. Garcia Saiz, G. Gregori, D. O. Gericke, J. Vorberger, B. Barbrel, R. J. Clarke, R. R. Freeman, S. H. Glenzer, F. Y. Khattak, M. Koenig, O. L. Landen, D. Neely, P. Neumayer, M. M. Notley, A. Pelka, D. Price, M. Roth, M. Schollmeier, C. Spindloe, R. L. Weber, L. van Woerkom, K. Wunsch, and D. Riley, Nat. Phys. **4**, 940 (2008).

[50]K. Nygaard, M. Hakala, S. Manninen, M. Itou, Y. Sakurai, and K. Hämäläinen, Phys. Rev. Lett. **99**, 197401 (2007).

[51]K. Nygaard, M. Hakala, T. Pylkkänen, S. Manninen, T. Buslaps, M. Itou, A. Andrejczuk, Y. Sakurai, M. Odelius, and K. Hämäläinen, J. Chem. Phys. **126**, 154508 (2007).

[52]J. A. Bradley, A. Sakko, G. T. Seidler, A. Rubio, M. Hakala, K. Hämäläinen, G. Cooper, A. P. Hitchcock, K. Schlimmer, and K. P. Nagle, Phys. Rev. A **84**, 022510 (2011).

[53]C. Fortmann, T. Bornath, R. Redmer, H. Reinholz, G. Röpke, V. Schwarz, and R. Thiele, Laser Part. Beams **27**, 311 (2009).

[54]C. Fortmann, A. Wierling, and G. Röpke, Phys. Rev. E **81**, 026405 (2010).

[55]A. Erba, M. Itou, Y. Sakurai, R. Yamaki, M. Ito, S. Casassa, L. Maschio, A. Terentjevs, and C. Pisani, Phys. Rev. B **83**, 125208 (2011).

[56]R. Redmer and G. Röpke, Contrib. Plasma Phys. **50**, 970 (2010).

[57]D. A. Chapman and D. O. Gericke, Phys. Rev. Lett. **107**, 165004 (2011).

[58]E. I. Moses, R. N. Boyd, B. A. Remington, C. J. Keane, and R. A. Ayat, Phys. Plasmas **16**, 041006 (2009).

[59]B. Nagler, U. Zastrau, R. R. Fäustlin, S. M. Vinko, T. Whitcher, A. J. Nelson, R. Sobierajski, J. Krzywinski, J. Chalupsky, E. Abreu, S. Bajt, T. Bornath, T. Burian, H. Chapman, J. Cihelka, T. Döppner, S. Düsterer, T. Dzelzainis, M. Fajardo, E. Förster, C. Fortmann, E. Galtier, S. H. Glenzer, S. Göde, G. Gregori, V. Hajkova, P. Heimann, L. Juha, M. Jurek, F. Y. Khattak, A. R. Khorsand, D. Klinger, M. Kozlova, T. Laarmann, H. J. Lee, R. W. Lee, K.-H. Meiwes-Broer, P. Mercere, W. J. Murphy, A. Przystawik, R. Redmer, H. Reinholz, D. Riley, G. Röpke, F. Rosmej, K. Saksl, R. Schott, R. Thiele, J. Tiggesbäumker, S. Toleikis, T. Tschentscher, I. Uschmann, H. J. Vollmer, and J. S. Wark, Nat. Phys. **5**, 693 (2009).

[60]S. Toleikis, T. Bornath, T. Döppner, S. Düsterer, R. R. Fäustlin, E. Förster, C. Fortmann, S. H. Glenzer, S. Göde, G. Gregori, R. Irsig, T. Laarmann, H. J. Lee, B. Li, K. H. Meiwes-Broer,

J. Mithen, B. Nagler, A. Przystawik, P. Radcliffe, H. Redlin, R. Redmer, H. Reinholz, G. Röpke, F. Tavella, R. Thiele, J. Tiggesbäumker, I. Uschmann, S. M. Vinko, T. Whitcher, U. Zastrau, B. Ziaja, and T. Tschentscher, J. Phys. B **43**, 194017 (2010).

[61] S. Toleikis, R. R. Fäustlin, L. Cao, T. Döppner, S. Düsterer, E. Förster, C. Fortmann, S. H. Glenzer, S. Göde, and G. Gregori, High Energy Density Phys. **6**, 15 (2010).

[62] S. M. Vinko, U. Zastrau, S. Mazevet, J. Andreasson, S. Bajt, T. Burian, J. Chalupsky, H. N. Chapman, J. Cihelka, D. Doria, T. Döppner, S. Düsterer, T. Dzelzainis, R. R. Fäustlin, C. Fortmann, E. Förster, E. Galtier, S. H. Glenzer, S. Göde, G. Gregori, J. Hajdu, V. Hajkova, P. A. Heimann, R. Irsig, L. Juha, M. Jurek, J. Krzywinski, T. Laarmann, H. J. Lee, R. W. Lee, B. Li, K. H. M. Broer, J. P. Mithen, B. Nagler, A. J. Nelson, A. Przystawik, R. Redmer, D. Riley, F. Rosmej, R. Sobierajski, F. Tavella, R. Thiele, J. Tiggesbäumker, S. Toleikis, T. Tschentscher, L. Vysin, T. J. Whitcher, S. White, and J. S. Wark, Phys. Rev. Lett. **104**, 225001 (2010).

[63] S. M. Vinko, O. Ciricosta, B. I. Cho, K. Engelhorn, H. K. Chung, C. R. D. Brown, T. Burian, J. Chalupsky, R. W. Falcone, C. Graves, V. Hajkova, A. Higginbotham, L. Juha, J. Krzywinski, H. J. Lee, M. Messerschmidt, C. D. Murphy, Y. Ping, A. Scherz, W. Schlotter, S. Toleikis, J. J. Turner, L. Vysin, T. Wang, B. Wu, U. Zastrau, D. Zhu, R. W. Lee, P. A. Heimann, B. Nagler, and J. S. Wark, Nature (London) **482**, 59 (2012).

[64] J. J. Rehr and R. C. Albers, Rev. Mod. Phys. **72**, 621 (2000).

[65] S. Huotari, K. Hämäläinen, S. Manninen, S. Kaprzyk, A. Bansil, W. Caliebe, T. Buslaps, V. Honkimäki, and P. Suortti, Phys. Rev. B **62**, 7956 (2000).

[66] C. Sternemann, M. Volmer, J. A. Soininen, H. Nagasawa, M. Paulus, H. Enkisch, G. Schmidt, M. Tolan, and W. Schülke, Phys. Rev. B **68**, 035111 (2003).

[67] S. Huotari, K. Hämäläinen, S. Manninen, C. Sternemann, A. Kaprolat, W. Schülke, and T. Buslaps, Phys. Rev. B **66**, 085104 (2002).

[68] C. Sternemann, T. Buslaps, A. Shukla, P. Suortti, G. Döring, and W. Schülke, Phys. Rev. B **63**, 094301 (2001).

[69] J. Chihara, J. Phys. F **17**, 295 (1987).

[70] J. Chihara, J. Phys.: Condens. Matter **12**, 231 (2000).

[71] A. Höll, R. Redmer, G. Röpke, and H. Reinholz, Eur. Phys. J. D **29**, 159 (2004).

[72] B. A. Remington, R. P. Drake, and D. D. Ryutov, Rev. Mod. Phys. **78**, 755 (2006).

[73] J. Korringa, Physica **13**, 392 (1947); W. Kohn and N. Rostoker, Phys. Rev. **94**, 1111 (1954).

[74] M. J. Cooper, P. E. Mijnarends, N. Shiotani, N. Sakai, and A. Bansil, *X-Ray Compton Scattering*, Oxford Series on Synchrotron Radiation (Oxford University Press, New York, 2004).

[75] P. Eisenberger and P. M. Platzman, Phys. Rev. A **2**, 415 (1970).

[76] A. Bansil, R. S. Rao, P. E. Mijnarends, and L. Schwartz, Phys. Rev. B **23**, 3608 (1981).

[77] S. B. Dugdale and T. Jarlborg, Solid State Commun. **105**, 283 (1998).

[78] M. P. Prange, J. J. Rehr, G. Rivas, J. J. Kas, and J. W. Lawson, Phys. Rev. B **80**, 155110 (2009).

[79] J. G. Norman, Mol. Phys. **31**, 1191 (1976).

[80] A. L. Ankudinov, B. Ravel, J. J. Rehr, and S. D. Conradson, Phys. Rev. B **58**, 7565 (1998).

[81] L. Lam and P. M. Platzman, Phys. Rev. B **9**, 5122 (1974).

[82] Y. Sakurai, J. Phys. Chem. Solids **60**, 905 (1999).

[83] P. Pattison, N. K. Hansen, and J. R. Schneider, Z. Phys. B **46**, 285 (1982).

[84] G. T. Seidler, M. Haave, J. I. Pacold, R. A. Gordon, and S. M. Heald (unpublished).